

POTENTIAL OF LOCK-IN INFRARED THERMOGRAPHY FOR THE RECOVERY OF DEFACED SERIAL NUMBERS

Ikwulono Unobe
College of Science and Engineering
Idaho State University
Pocatello, Idaho, 83209,
USA

¹unobikwu@isu.edu

Lisa Lau
College of Science and Engineering
Idaho State University
Pocatello, Idaho,
83209, USA

John Kalivas
College of Science and Engineering
Idaho State University
Pocatello, Idaho,
83209, USA

Andrew Sorensen
College of Science and Engineering
Idaho State University
Pocatello, Idaho,
83209, USA

Rene Rodriguez
College of Science and Engineering
Idaho State University
Pocatello, Idaho,
83209, USA

Abstract— Infrared thermography is an evolving approach useful in nondestructive evaluation of materials for industrial and research purposes. A two stage method is proposed here to utilize infrared thermography to recover defaced serial numbers. The first stage involves employing the lock-in thermography technique to develop phase images which are less susceptible to environmental conditions and uneven heating than raw thermal images. The second stage involves the application of principal component analysis (PCA), a multivariate technique that transforms a dataset of possibly correlated variables into a set of new uncorrelated variables on the phase images to enhance subtle variations of temperature gradient across the surface under investigation. This two stage approach has the advantage of utilizing the benefits of lock-in thermography as well as the potential of PCA as an analytical tool to recover defaced serial numbers. The results are presented for a stainless steel plate stamped with several numbers and then defaced.

Keywords—infrared thermography; principal component analysis; lock-in; phase; score image; serial numbers

I. INTRODUCTION

Stamp marks provide a means of unique identification for a range of items notably firearms and automobiles. However, these are regularly erased for criminal activities using a variety of techniques including filing, grinding, over-stamping, etc. [1]. The stamping of serial numbers onto metals causes a permanent change in shape primarily due to the inability of the molecular crystalline structure to resist the induced stress of stamping. This leads to an alteration of the local crystalline structure extending to some depth below the stamped mark in a region called the zone of plastic strain [2]. The depth of this zone is dependent on several factors including metal type, size and shape of the stamp and the force used to produce the marking. Due to the stress induced alterations in its microstructure, the zone of plastic strain has physical and chemical properties differing from those of the original metal. These include an increase in hardness and electrical resistivity, decrease in ductility and yield stress, as well as changes in its magnetic properties and chemical potential.

A nondestructive technique which has proven useful in the detection of subsurface defects in metals and could be used in

restoration of defaced serial numbers is infrared thermal imaging. Infrared radiation refers to energy in the region of the electromagnetic radiation spectrum at wavelengths longer than those of visible light, but shorter than those of microwaves. Infrared thermal imaging is sensitive to variations in thermal conductivity within a material, caused by the presence of local regions of plastic strain from the stamping. It involves the application of heat to a material surface to raise its temperature substantially albeit to a nondestructive level. Then by observing the propagation of the heat through the material, it is possible to detect regions of plastic strain on the surface where the temperature gradients differ from the rest of the surface. An IR camera is used to capture the temperature profile of the metal surface.

The physical models that help guide the experimental studies for infrared thermal imaging are based on a heat conduction model which describes the temperature distribution in a heated material as obeying the general one dimensional heat transfer equation [3].

$$\frac{d^2T}{dx^2} - (\rho c/k) \frac{dT}{dt} = 0 \quad (1)$$

where, T is the temperature, x is the perpendicular distance from the surface of the heated sample, t is the time and ρ , c and k are the density, heat capacity and thermal conductivity respectively.

However, when defects are present in the material, propagation of the thermal wave in the defective regions differ from the rest of the material and thus there are multiple conduction equations governing the heat flow.

$$\frac{d^2T_0}{dx^2} - (\rho_0 c_0/k_0) \frac{dT_0}{dt} = 0 \quad (2)$$

$$\frac{d^2T_1}{dx^2} - (\rho_1 c_1/k_1) \frac{dT_1}{dt} = 0 \quad (3)$$

where the subscript 0 represents the clean region and 1 represents the defaced areas.

This project was supported by Award No. 2013-R2-CX-K012, awarded by the National Institute of Justice, Office of Justice Programs, U.S. Department of Justice. The opinions, findings, and conclusions, or recommendations expressed in this exhibition are those of the authors and do not necessarily reflect those of the Department of Justice.

From (2) and (3), even though the temperature of both regions may initially be the same, their temperature gradients will vary since the thermal conductivity and perhaps the density and heat capacities of the two regions will be dissimilar. Thus by monitoring the temperature gradient across a material's surface, the velocity or phase of a thermal wave passing through it or the temperature distribution across its surface, the deformed regions should be detectable.

II. FINITE ELEMENT MODELING

Finite element analysis (FEA) is a numerical technique that can be used to model the behavior of an object under defined conditions. The model designed for this study assumed 3D heat transfer conditions within a homogenous stainless steel plate [4]. The thermal and geometrical parameters were defined for this model to emulate those of stainless steel (AISI 304). Boundary conditions were defined to include heat transfer by conduction. The finite element analysis was carried out using ANSYS®.

The finite element model developed is shown in Fig. 1. This is a stainless steel plate with static force applied to simulate stamping pressures used to impress a number. Fig. 2 shows the plastic strain distribution around the number stamped into a plate. This strain is resultant from the distorted crystalline structure of the material due to the force of stamping and is concentrated around the area of the stamped number.

Fig. 3 shows the plastic strain distribution on the plate after 3 mm of material was removed from the surface, replicating the defacing of serial numbers process. The plastic strain at this depth is more widely distributed and the number can no longer be uniquely identified at room temperature.

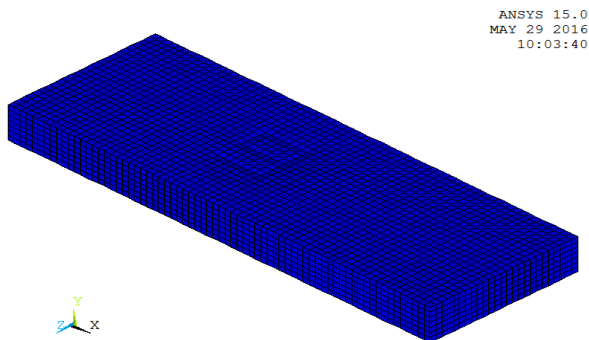


Fig. 1: Meshed FE model with stamped number

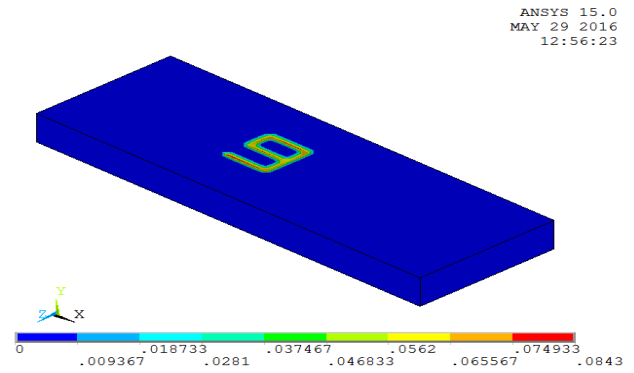


Fig. 2: Plastic Strain distribution on surface of FE model

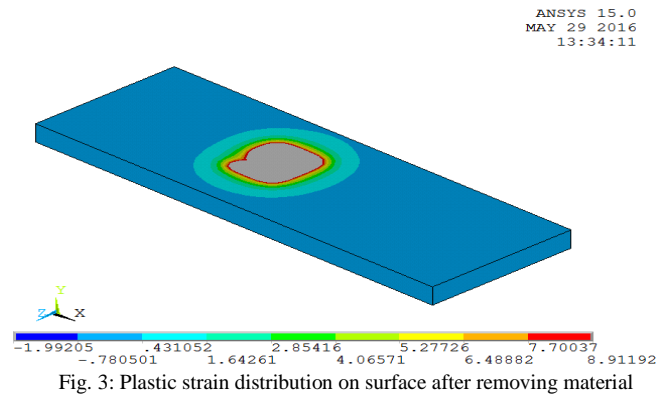


Fig. 3: Plastic strain distribution on surface after removing material

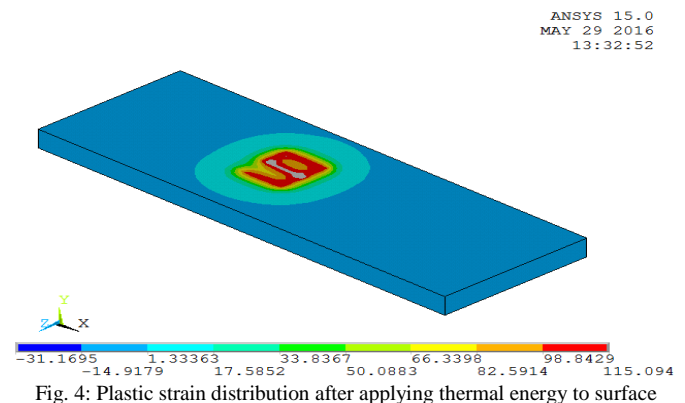


Fig. 4: Plastic strain distribution after applying thermal energy to surface

Fig. 4 shows the plastic strain distribution after the application of heat flux to the surface. The heat conduction through the sample is uneven across the surface due to the plastic strain around the removed number and thus, the temperature in this region is significantly higher than that on the rest of the surface allowing for identification of the number that was removed from the region. This corroborates the posited material behavior under thermal energy.

III. EXPERIMENTAL SETUP AND DATA COLLECTION

The experimentation system consists of an infrared camera, a function generator and thermal energy source as shown in Fig. 5. The primary thermal energy source, a 5W Ar-ion cw laser, operating in all-lines mode, is chopped with a Uniblitz mechanical shutter to apply pulsed energy to the sample. A

FLIR SC6700 IR camera is used to collect thermal images of the sample surface and a Stanford Research Systems 15MHz function generator synched with the camera is used to control the pulse rate of energy from the laser. During the experiments, the defaced surface of the sample was heated using the laser. The temperature distribution on the heated surface was monitored using the infrared camera with images collected at a sampling frequency of 32 frames per cycle.

Experiments were performed on a stainless steel plate stamped with several numbers as shown in Fig. 6. The sample was originally 6.35 mm thick. Each number was progressively shaved off with the area around each successive number removed 0.02 mm depth beyond the previous. The first number on the plate is left visible to serve as control. Fig. 7 shows the defaced sample. After the defacing, it is quite impossible to identify the numbers that were present before the material was removed.

IV. IMAGE PROCESSING AND RESULTS

A two stage image processing scheme is utilized for this study. In the first stage, the raw thermal data is transformed into phase and amplitude images using the lock-in correlation procedure [5]. A dataset of phase images is then subjected to principal component analysis to enhance visibility of the defaced numbers.

A. Lock-In Infrared Thermography

Lock-in Infrared Thermography involves the application of a periodic thermal energy wave to the surface of a material.

This wave is allowed to propagate through the material. This heat flow will be affected by possible thermal conductivity differences across the surface of the material and as such, changes in the phase of the wave will be experienced as it propagates through [6]. A major advantage of LIT over other thermography techniques is that the phase images are insensitive to uneven heating and local emissivity variations which are concerns in using other thermal imaging techniques.

The principle of Lock-in thermography is described by [5]. A sinusoidal energy wave is induced into the surface of a sample and the IR camera is used to collect thermal images of the sample surface over the entire period of the pulsed wave. A 2 channel image correlation procedure involving multiplying each collected image by two sets of weighting factors, and then summing together all the results is used to develop one in-phase image (0°) and a quadrature (-90°) image.

$$S^{0^\circ} = \frac{1}{n} \sum_{k=1}^n \sin(t) * F_k(t) \quad (4)$$

$$S^{90^\circ} = \frac{1}{n} \sum_{k=1}^n -\cos(t) * F_k(t) \quad (5)$$

where n is the number of frames per lock-in period, F_k is the image collected at time t and $\sin(t)$ and $\cos(t)$ are the weighing factors.

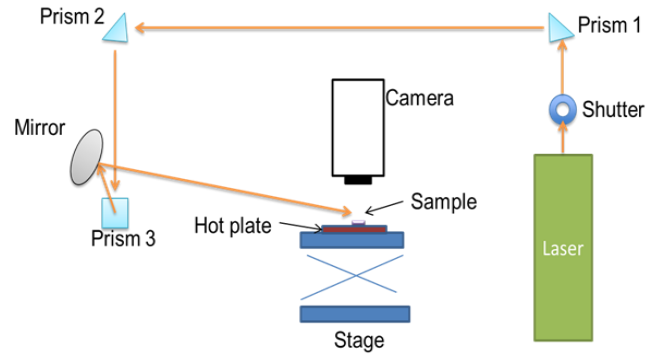


Fig. 5: Experimental Setup

A phase independent amplitude image A , and a signal phase image ϕ are then generated using (6) and (7):

$$A = \sqrt{(S^{0^\circ})^2 + (S^{90^\circ})^2} \quad (6)$$

$$\phi = \tan^{-1} \left(\frac{S^{90^\circ}}{S^{0^\circ}} \right) \quad (7)$$

The phase image is more useful for analyzing subsurface defects as it is less susceptible to environmental conditions than the thermal images, thus giving better surface temperature signals.

A major drawback of lock-in thermography is blind frequencies i.e. pulsing frequencies at which the contrast between clean areas and defective areas is minimal. Defect detection in phase images developed at these frequencies is usually difficult and thus, such frequencies need to be avoided. To address this shortcoming, phase difference plots can be developed as the difference between a defective area and a clean area [7].

$$\Delta\phi(x, y) = \phi_d(x, y) - \phi_s(x, y) \quad (8)$$

where, $\Delta\phi(x, y)$ is the phase difference of the pixel (x, y) , $\phi_d(x, y)$ is the phase of a pixel in the defect area and $\phi_s(x, y)$ is the phase of a pixel in a sound area.

Phase images were calculated in this study for several complete heating periods. Fig. 8 shows the phase difference plots for the different numbers on the sample. The phase differences were calculated as the difference between the phase values within the region where the number previously existed and average phase values of a clean area for various pulsing frequencies. From this figure, it can be observed that while there is no blind frequency for the numbers, suboptimal frequencies that will give the least contrast are 250 mHz and 1000 mHz. Optimal frequencies for all the numbers are observed to be 0.05 mHz to 0.015mHz.

B. Image Analysis

Image analysis was carried out primarily using principal component analysis (PCA). PCA reduces a dataset of images



Fig. 6: Stainless steel plate stamped with several numbers



Fig. 7: Plate with numbers removed

into a number of factorials (principal components) each of which is a linear combination of the original dataset and are orthogonal to each other. These principal components account for the variability in the data with the first accounting for most of the variability and as such has the largest eigenvalue associated with it [8-9].

Fig. 9 shows the IR thermal image of a clean stainless steel surface left intact with no number stamped into it. The image is comparable to those shown in Fig. 10 of the areas around the defaced numbers. As with the sample at room temperature, the numbers removed cannot be uniquely distinguished from a clean surface in the infrared thermal images. The imaged areas around the numbers all have equal number of rows but differing number of columns to compensate for changes in the widths of the stamps used for each number.

Phase images were developed from these thermal images over a cycling period. Figs. 11 and 12 show phase images developed from the thermal images collected for the clean region and defaced numbers respectively. Although the phase images have effectively cleaned up the thermal images, removing such unwanted features as inhomogeneous illumination as well as possible environmental effects, it is still impossible to identify the serial numbers removed from the images.

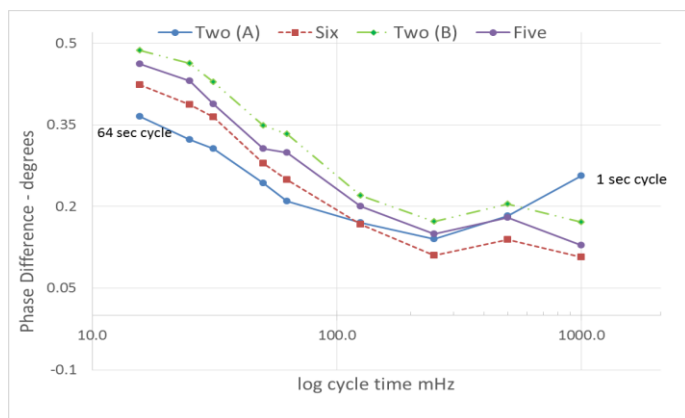


Fig. 8: Phase Difference plots for the defaced numbers

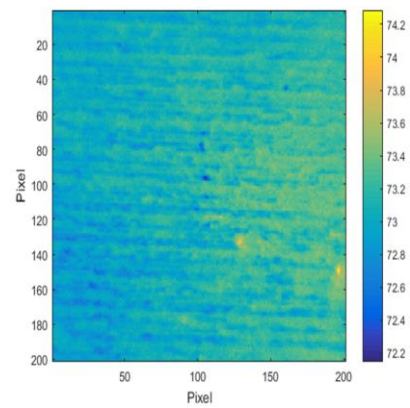


Fig. 9: IR thermal image of clean area (200 x 200 pixels)

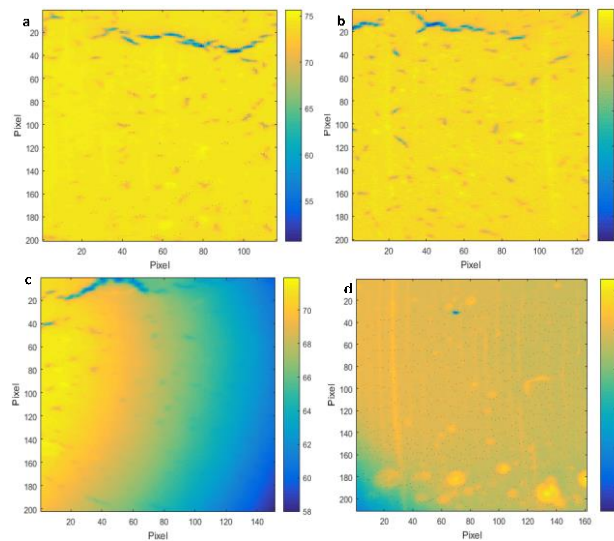


Fig. 10: IR thermal images of area around (a) Number 6 (210x 116 pixels) (b) Number 2 (210x152 pixels) (c) Number 5 (210x151 pixels) and (d) Number 0 (210 x 161 pixels)

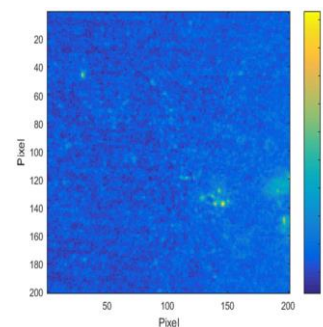


Fig. 11: Phase image of clean area

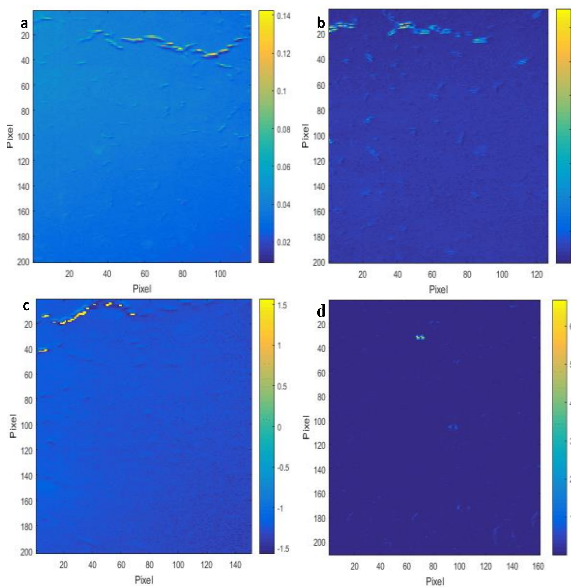


Fig. 12: Phase image at 50 mHz of area around (a) Number 6 (b) Number 2 (c) Number 5 and (d) Number 0

Principal component analysis was used to develop score images from a dataset of phase images to further enhance the visibility of subsurface features. These score images are reconstructions of the principal component vectors into images which display the variability in intensity of the different pixels over time. Table 1 shows the percent variance of information explained in each PC. As by convention, PC1 explains the most amount of variance and the other PCs explain some of the remaining variance present in decreasing order.

Fig. 13 presents the score images from the clean undefaced region. The score images were produced by applying principal component analysis to each pixel of the set of phase images developed. PC1 is responsible for 99% of the variance within the images. PC 2 through PC 15 is responsible for the remaining 1% of the variance. The score images show no identifiable structure although with some random high intensity areas due to surface roughness of the sample. This is expected as no crystalline deformation exists within the sample in this region. Fig. 14 shows the score images from the area around the number 6. The first principal component PC1 is responsible for 98% of the variance and PC 2 through PC 15 for the remaining 2%. However, unlike for the clean area, one of the score images (PC13) shows defined intensity contrast localized around the section where the number previously existed. This PC although only explaining 0.0003% of the variance, due in part to the surface roughness creating discrepancies in the thermal gradient of pixels across the surface and thus partially masking the plastic strain, still shows enough structure to distinguish the zone of plastic strain.

Table 1: Percent Variances for each PC

	Percent Variance (%)
--	----------------------

PC	Clean area	Six	Two	Five	Zero
1	99.0328	98.5497	82.291	99.855	48.6725
2	0.56392	1.0724	16.8583	0.082009	8.9673
3	0.25804	0.22185	0.70217	0.037486	5.5631
4	0.11516	0.099338	0.062361	0.012517	5.4441
5	0.010811	0.031153	0.028275	0.005988	4.753
6	0.0064361	0.014198	0.016198	0.00169	4.4526
7	0.0027451	0.005206	0.012695	0.001264	3.7963
8	0.0022548	0.002654	0.00737	0.001006	3.6741
9	0.0018653	0.000998	0.00548	0.000844	3.242
10	0.0013557	0.000854	0.004638	0.00063	2.8108
11	0.0012379	0.00058	0.003418	0.000417	2.5601
12	0.00085649	0.000424	0.002901	0.000365	2.2362
13	0.00079091	0.00026	0.002077	0.000288	1.9693
14	0.0006633	0.000218	0.001644	0.000246	1.1534
15	0.00056045	0.000173	0.001566	0.000234	0.7053

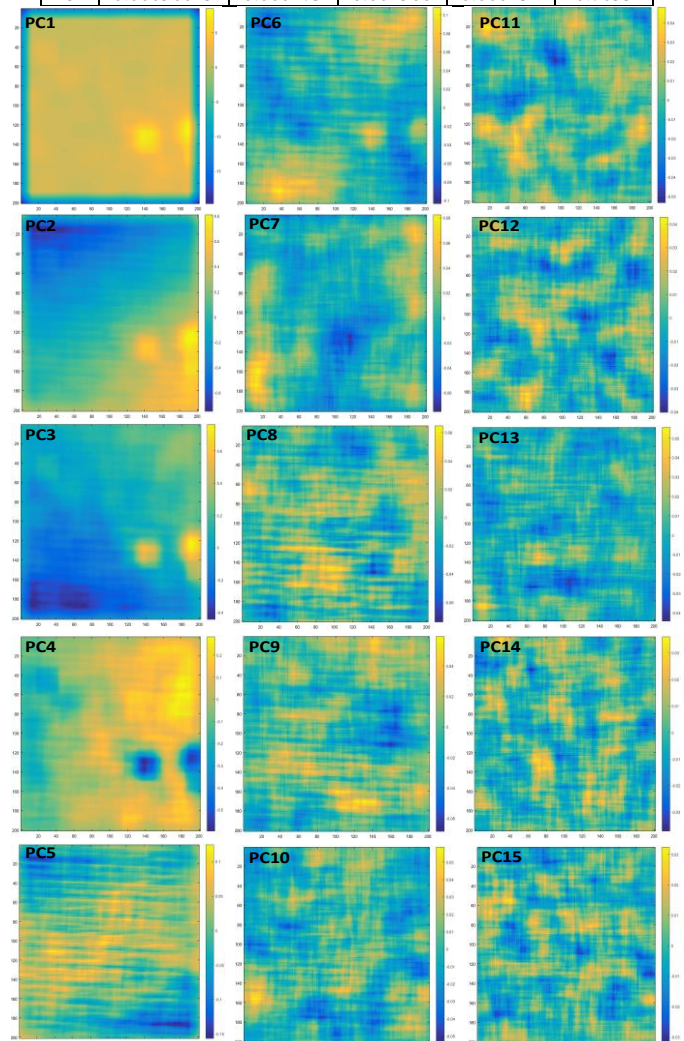


Fig. 13: PC score images of clean area

This highlights an advantage of PCA in recognizing even small variances that may exist across pixels in an image.

Figs. 15 through 17 similarly show the refolded score images from the pixel by pixel principal component analysis of the regions around the numbers 2, 5 and 0 respectively. From Fig. 15, PC 11 shows some contrast in the region where the number existed. This PC accounts for only 0.003% of the variance. Likewise, PC 10 of Fig. 16 shows some contrast in intensity allowing for possible identification of the number that was removed. PC 1 of Fig. 17 accounting for 49% of the variance shows intensity contrast to possibly identify the number that previously existed there. The disparity in the PC best identifying the thermal gradient variation for the different numbers is due to the surface conditions of the areas. The surface roughness from the machining process is random over each area with no defined pattern. As such, the variance in the scores differs for each area accounting for the change in the PC best explaining the thermal gradient variation.

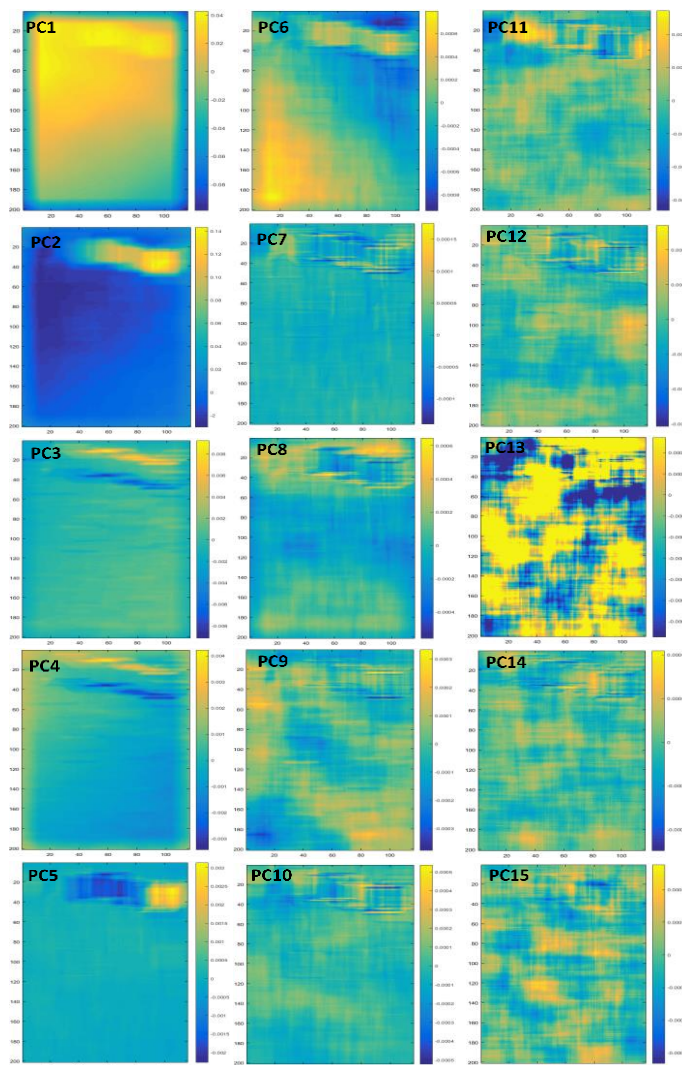


Fig. 14: Refolded PC score images of the area around the defaced number 6 with PC 13 showing the best representation of the number

V. CONCLUSION

A two stage process involving the use of infrared thermography and principal component analysis (PCA) as a nondestructive technique for recovering defaced serial numbers is proposed in this study. As observed in [7], the LIT technique has been successfully utilized in detecting subsurface features of objects. Combining this technique with PCA, useful for detecting inherent relationships within a dataset has proven to effectively identify thermal gradient differences within the regions exposed by the defaced numbers. This preliminary study has focused on the viability of such a methodology. Further studies are being conducted in a parametric manner to identify the best experimental conditions such as optimal cycle time and input thermal energy for the restoration process.

Some image processing techniques which would further improve contrast in the score images to improve character recognition are also being investigated.

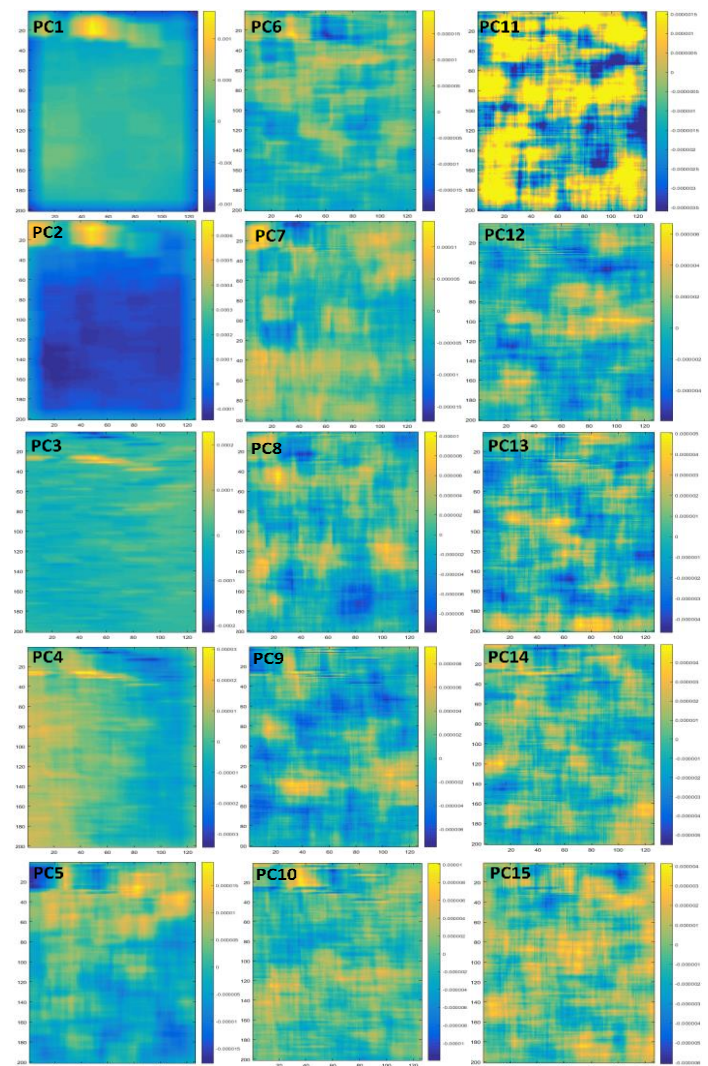


Fig. 15: Refolded PC score images of the area around the defaced number 2 with PC 11 showing the best representation of the number

ACKNOWLEDGMENT

The authors would like to thank Miles Whiting of ISU Machining services for creating the samples as well as Royce Martin of ISU Electronic services for helping with the equipment.

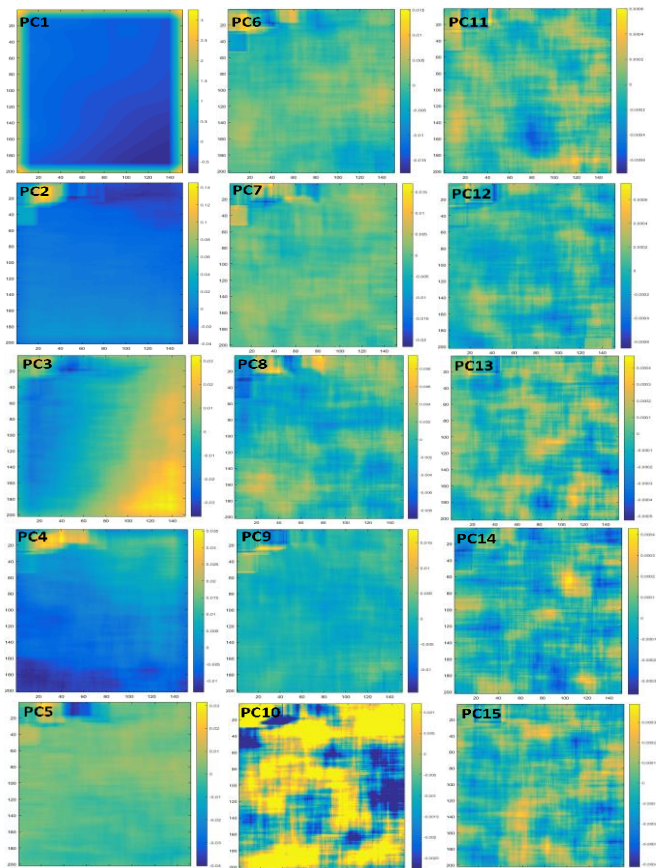


Fig. 16: Refolded PC score images of the area around the defaced number 5 with PC 10 showing the best representation of the number

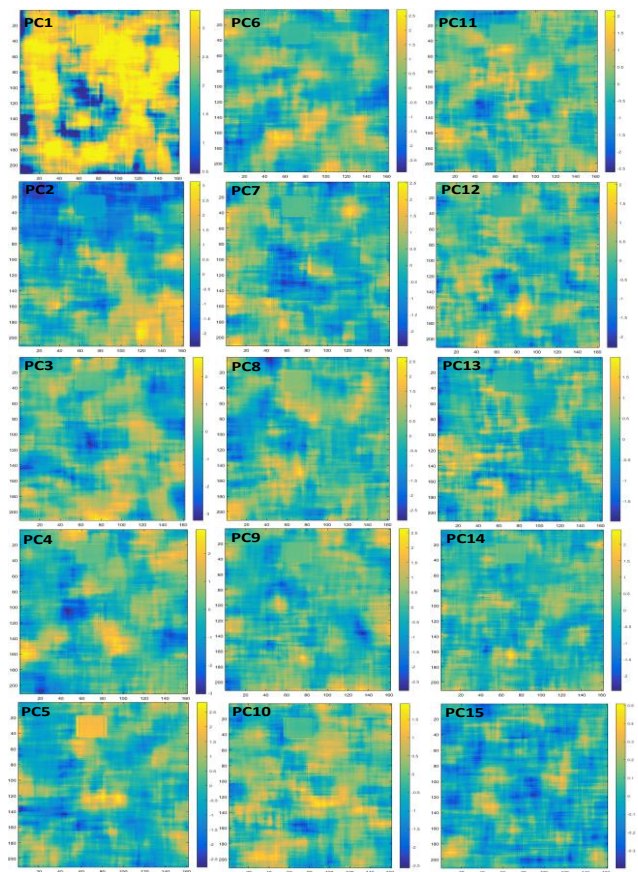


Fig. 17: Refolded PC score images of the area around the defaced number 0 with PC 1 showing the best representation of the number

REFERENCES

- [1] Nickolls, Lewis C. *The scientific investigation of crime*. Butterworth, 1956.
- [2] Polk, Donald E., and B. Giessen. "Metallurgical aspects of serial number recovery." *AFTE Journal* 21.2 (1989): 174-181.
- [3] Cramer, K. Elliott, Patricia A. Howell, and Hazari I. Syed. "Quantitative thermal imaging of aircraft structures." *SPIE's 1995 Symposium on OE/Aerospace Sensing and Dual Use Photonics*. International Society for Optics and Photonics, 1995.
- [4] Ranjit, Shrestha, and Won Tae Kim. "Detection of subsurface defects in metal materials using infrared thermography; image processing and finite element modeling." *Journal of the Korean Society for Nondestructive Testing* 34.2 (2014): 128-134.
- [5] Breitenstein, O., and M. Langenkamp. "Lock-in Thermography: Basics and Use for Evaluating Electronic Devices and Materials (Series in Advanced Microelectronics)." (2003): 29-32.
- [6] Liu, Hui, et al. "Effect of modulation frequency on detecting defects of metal plates using infrared lock-in thermography." 4th International Symposium on Advanced Optical Manufacturing and testing technologies: Optical Test and Measurement Technology and Equipment. International Society for Optics and Photonics, 2009.
- [7] Choi, Manyong, et al. "Quantitative determination of a subsurface defect of reference specimen by lock-in infrared thermography." *Ndt & E International* 41.2 (2008): 119-124.
- [8] Geladi, Paul, and Hans F. Grahn. *Multivariate image analysis*. John Wiley & Sons, Ltd, 1996.
- [9] Jackson, J. Edward. *A user's guide to principal components*. Vol. 587. John Wiley & Sons, 2000